Minerals Engineering 209 (2024) 108621

Contents lists available at ScienceDirect

Minerals Engineering

journal homepage: www.elsevier.com/locate/mineng

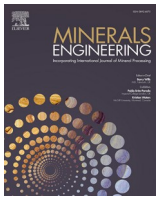

A systematic study on gelatinization efficiency of starch by NaOH for enhanced hematite depression

Elaine Cristina Andrade [a], Saeed Chehreh Chelgani [b,*], Laurindo de Salles Leal Filho [a]

[a] Department of Mining and Petroleum Engineering, Polytechnic School, University of São Paulo, Av. Professor Mello Moraes, 2373, CEP 05508-900, São Paulo, SP, Brazil

[b] Minerals and Metallurgical Engineering, Department of Civil, Environmental and Natural Resources Engineering, Swedish School of Mines, Luleå University of Technology, Luleå, Sweden

ARTICLE INFO

Keywords:
Hematite reverse flotation
Depression
Starch
Gelatinization
Hydrodynamic diameter

ABSTRACT

Starch is a traditional depressant for hematite beneficiation by cationic reverse flotation separation from silicates. Alkali or thermal gelatinization must be used to prepare starch and promote its dissolution in water. In industry, gelatinization is typically carried out using sodium hydroxide at room temperature at different starch/NaOH mass ratios (SNMR). Surprisingly, no investigation has systematically studied the optimum SNMR for boosting hematite depression. This work examined the influence of starch gelatinization under various SNMR (3:1, 5:1, 7:1, and 9:1) on hematite depression (at pH = 10.5, 22 °C) by exploring flotation response (R), contact angle (θ), induction time (τ), hydrodynamic diameter (d_H) of starch macromolecules, total energy of interaction starch/hematite (G^{TOT}), based on its two components: the attractive Lifshitz-van der Waals energy (G^{LW}) and attractive/repulsive electrostatic energy (G^{EL}). Flotation test results indicated that SNMR = 5:1 promoted the lowest hematite recovery (14.8 %), coupled with the highest induction time (τ = 55 ms) and the lowest contact angle ($\theta = 11^{\circ}$). The hydrodynamic diameter (d_H) of macromolecules in solutions prepared under different SNMR was determined by Dynamic Light Scattering, showing three peaks: amylopectin ($350 < d_H < 420$ nm), amylose ($50 < d_H < 100$ nm) and debris from gelatinization ($d_H \sim 5000$ nm). Since the latter only occurred in solutions prepared under SNMR of 7:1 and 9:1, deficient hematite depression might be caused by incomplete gelatinization. As amylopectin is the starch component that is responsible for its depressant ability, larger amylopectin macromolecules (d_H = 411 nm) found in solutions prepared at SNMR = 5:1 contrast with smaller macromolecules (d_H = 353 nm) produced at SNMR = 3:1. Considering starch macromolecules as a sphere, and hematite's surface as a plane; G^{LW}, G^{EL}, and G^{TOT} were calculated in function of the sphere/plane separation distance (2 nm < H < 20 nm). G^{LW} was determined based on the assessment of the Hamaker constant of the starch/water/hematite system (2.9×10^{-20}J < A_{132} < 3.3×10^{-20}J), whereas G^{EL} was determined based on the zeta potential of starch (−2mV < ζ_1 < −4mV) and hematite (ζ_2 = −29 mV). G^{TOT} for starch gelatinized at SNMR = 5:1 (-502.9×10^{-21} J) is greater than G^{TOT} for starch prepared at SNMR = 3:1 (-468.8×10^{-21} J) and SNMR = 7:1 (-469.0×10^{-21} J), at a confidence level of 95 %. These results corroborate the more intensive hematite depression by starch prepared at SNMR = 5:1 compared to the other values explored by this study.

1. Introduction

The reverse cationic flotation separation of hematite from silicates in a basic medium has been successfully used in Brazil for over 40 years. In this particular case, long-chain ether amine ($R–O–CH_2–NH_3^+$) acts as a collector for silicates, whereas gelatinized corn starch acts as a hematite depressant (Deng et al., 2019; Kar et al., 2013; Li et al., 2022; Nykänen et al., 2020; Shrimali et al., 2016; Shrimali and Miller, 2016; Silva et al., 2021, 2016, 2019; Yang and Wang, 2019; Zhang et al., 2022). Starch is a natural biopolymer (polysaccharide) composed predominantly of amylose (AM) and amylopectin (AP) in contents that depend largely on the starch source; for instance, corn starch bears 25 % of AM and 75 % of AP, whereas industrial starches contain 20–30 % of AM, 70–80 % of AP and <1 % of lipids, proteins, phosphorus and fibers (Asimi Neisiani et al., 2023; Kar et al., 2013; Silva et al., 2016).

AP is the most important starch component since it is responsible for

* Corresponding author.
E-mail address: saeed.chelgani@ltu.se (S.C. Chelgani).

https://doi.org/10.1016/j.mineng.2024.108621
Received 2 December 2023; Received in revised form 9 February 2024; Accepted 10 February 2024
Available online 15 February 2024

Table 1
Flotation response of hematite versus starch type, dosage, and gelatinization.

Type	SNMR or gelatinization method	Dosage	Collector type and dosage	pH	Recovery of hematite	References
NS: 27/73 G50: 50/50	Alkali plus thermal gelatinization	1.5 g/L	Dodecyl ammonium chloride 4×10^{-3} M	7.2	NS: 30 % G50: 37 %	(Yang and Wang, 2018)
SS: 25/75 CS: 28/70 RS: 0/- PS: 20/73	CS, RS, and PS were dissolved in slightly warm water, while SS was prepared in cold water	400 g/t	Dodecylamine 48 g/t	6.5	SS: 9 % CS: 9 % RS: 10 % PS: 12 %	(Kar et al., 2013)
Corn starch	SNMR = 5:1	50 mg/L 100 mg/L	Mono ether amine 100 mg/L	10.5	40 % 37 %	(Shrimali et al., 2018)
Corn starch	SNMR = 5:1	500–1000 mg/L	Mono ether amine 50 mg/L	10.5	<10 %	(Rohem Peçanha et al., 2019)
Corn starch	SNMR = 10:1 plus heating in a water bath at 95 °C with stirring for 1 h	15 mg/L 30 mg/L 45 mg/L 60 mg/L	Dodecylamine 2×10^{-4} M	10.5	55 % 47 % 35 % 23 %	(Zhang et al., 2022)
NS: 27/73 WS: 0/100 G50: 50/50	SNMR = 4:1 plus heating until starch solution became transparent	140 mg/L	Dodecylamine 30 mg/L	10.0	NS: 1.0 % WS: 0.5 % G50: 19.9 %	(Yang et al., 2023)
Corn starch: 39/49 Sorghum starch: 25/62	SNMR = 3.7:1	5–40 mg/L	Mono ether amine 20 mg/L	10.5	Corn starch: 8–24 % Sorghum starch: 7–12 %	(Silva et al., 2019)
NS: 27/73 WS: 0/100 G50: 50/50 G80: 80/20	Starches solutions were prepared at 65 °C and pH 13 under a stirring rate of 400 rpm	1.5 mg/L	Dodecyl ammonium chloride 4×10^{-4} M	8.5	NS: 4 % WS: 4 % G50: 11 % G80: 27 %	(Yang et al., 2017)
Starch Amylose Amylopectin	SNMR = 4:1	5 mg/L	Dodecylamine hydrochloride 5×10^{-5} M	10.0	Starch: 17 % Amylose: 35 % Amylopectin: 7 %	(Pinto et al., 1992)
Corn starch: 39/49 Millet starch: 21/67 Sorghum starch: 25/62	SNMR = 3.7:1	5–40 mg/L	Mono ether amine 20 mg/L	10.5	Corn starch: 4.5–0.9 % Millet starch: 1.7–0.4 % Sorghum starch: 2.1–0.7 %	(Silva et al., 2021)

NS = normal starch, G50 = gelose 50, G80 = gelose 80, SS = soluble starch, CS = corn starch, RS = rice starch, PS = potato starch, WS = waxy starch.

the functional properties of starches in solution. In other words, it is sufficient to form a granule, as occurs in some genetically modified waxy starches (Asimi Neisiani et al., 2023; Cornell, 1963; Fu et al., 2022; Kar et al., 2013; Laskowski et al., 2007). Moreover, AP responds to the starch's ability to depress hematite and other Fe-bearing minerals (Asimi Neisiani et al., 2023; Iwasaki, 1965; Pinto et al., 1992; Silva et al., 2017; Yang et al., 2017; Yang and Wang, 2019, 2018). The physicochemical characteristics of starch aqueous dispersions influence their depressant ability, e.g., AM/AP content, branching level, solubility, and acidity (Asimi Neisiani et al., 2023; Bello-Perez et al., 1996; Li et al., 2022; Rolland-Sabaté et al., 2011; Shrimali and Miller, 2016; Tang et al., 2022; Yang and Wang, 2018; Zhang et al., 2022). In other words, to understand the interaction between starch (AP) and Fe-oxide minerals, one must account for the existence of polar groups (hydroxyl, carboxyl and carbonyl) along the molecular structure of starch (Kar et al., 2013; Roger et al., 1999; Yang et al., 2023), the fully hydroxylated surface of Fe-oxide minerals in aqueous basic medium (Kar et al., 2013; Roger et al., 1999; Yang et al., 2023) and a strong chemical interaction (surface complexation) between them (Moreira et al., 2017; Weisseborn et al., 1995).

Since starch granules are insoluble in cold water, they must be treated by alkaline and/or thermal gelatinization to promote their dissolution before being used as a depressant in froth flotation. The preparation method, which invariably requires gelatinization of this biopolymer, influences its interaction with the mineral surface and its performance as a depressant agent. In industry, gelatinization is usually carried out by using sodium hydroxide at different "starch: NaOH" mass ratios (SNMR) at room temperature (Iwasaki, 1965; Nykänen et al., 2020; Shrimali and Miller, 2016; Silva et al., 2021, 2017, 2016, 2019; Tang et al., 2022, 2016; Tang and Liu, 2012; Yang et al., 2017; Yang and Wang, 2018). Moreira et al. (2017) studied the interaction of starch macromolecules (AP) and hematite, indicating that not only does the gelatinization process solely expose OH groups to interact with Fe-hydroxylated sites that exist on the surface of hematite but also allows the formation of other functional groups (C=O, COOH) via oxidation which can interact with the same hematite's surface sites as well (Moreira et al., 2017). The preferential adsorption of AP species onto different hematite surface planes: (1120) > (1100) > (0001) was also

reported. This sequence is supported by the density of the Fe-hydroxylated surface sites available to interact with starch (Félix et al., 2022). Although various flotation processes (Table 1) utilize starch prepared under different SNMR to accomplish hematite depression through the reverse cationic flotation of silicates (mainly quartz), surprisingly, no systematic investigation has been conducted to explore the effects of SNMR on the starch adsorption on the hematite surface through its reverse flotation separation.

Dynamic light scattering (DLS) is the most common technique to characterize the dimension and behavior of starch macromolecular components in solution, such as size, polydispersity, and hydrodynamic behavior. Due to Brownian motion, the particles dispersed in a liquid move randomly in all directions and assume new positions within the scattering field at any moment (time scale in ms). This way, particles scatter radiation with differing incident phases due to their position at several particle-detector distances (Bello-Perez et al., 1996; Iselau et al., 2016; Ragheb and Nobbmann, 2020; Roger et al., 1999; Rolland-Sabaté et al., 2011). Roger et al. (1999) used DLS and indicated that, as the treatment time increased, the hydrodynamic radius (R_H) decreased for all starch samples, reflecting the macromolecular degradation during the solubilization process. It was also observed that in the distribution of relaxation times as a function of R_H, only one broad peak was observed for the AM-free sample (Roger et al., 1999). They highlighted the possibility of drawing a picture that depicts a bimodal size distribution for AM and AP molecules in different size ranges (Roger et al., 1999).

Rohem Peçanha et al. (2019) studied the interaction between mineral particles (quartz, hematite) and colloidal corn starch (gelatinized with SNMR = 5:1) using the classical DLVO theory, following the same rationale used by other authors to approach the interaction between microorganisms and minerals (Botero et al., 2008). Accordingly, as shown by Eq. (1), the total interaction energy (G^{TOT}) between colloidal starch and hematite is the sum of Lifshitz-van der Waals (G^{LW}) and electrostatic (G^{EL}) interaction energies. If the sign of G^{TOT} is negative ($G^{TOT} < 0$), the interaction is favorable (attraction), whereas $G^{TOT} > 0$ indicates repulsion. In addition, the more negative G^{TOT} is, the greater the attraction between colloidal starch and hematite.

$$G^{TOT} = G^{LW} + G^{EL} \quad (1)$$

As Hunter and White (1987) maintained, the contribution given by G^{LW} is due to microscopic attractive forces originating from permanent and induced electrical interactions between two or more atoms/molecules existing in the structure of two approaching particles, such as colloidal starch and hematite. In addition, the contribution given by G^{EL} accounts for Colombian attraction/repulsion between approaching particles (colloidal starch and hematite) due to electrical double-layer interactions. Based on a fundamental approach, this study examined the effects of various SNMR on the ability of starch to inhibit the flotation of hematite (contact angle, induction time, and flotation recovery) vis-à-vis the size of macromolecules (via DLS) and zeta potential (electrophoretic mobility) of hematite and starch colloidal particles (macromolecules), as well as the interaction energy starch/hematite (effective Hamaker constant A_{132}, G^{LW}, G^{EL}, and G^{TOT}).

2. Materials and methods

2.1. Minerals and materials

Vale S.A. supplied a 200 kg naturally rich sample of hematite (Carajás - Brazil). Some chunks of hematite from the raw sample were handpicked, embodied in resin, polished, and carefully stored for contact angle measurements and induction time. The remaining sample was crushed and ground −150 μm in the laboratory. The product was wet sieved to reject the slimes (−20 μm fraction). Wet screening assessed the particle size distribution of the −150 +20 μm fraction (P_{80} = 106 μm). Since this size fraction meets the market specification for pellet feed (−150 μm), it was used for the flotation experiments. The −20 μm size fraction (d_{32} = 6.92 μm) was used for zeta potential measurements. Mineralogical and chemical analyses of the flotation feed were performed by X-ray diffraction "XRD" (Malvern Panalytical, Empyrean) and X-ray fluorescence "XRF" (Malvern Panalytical, Zetium), respectively. Based on the XRF-XRD analyses (Table 2), the sample contained 68.9 % of Fe (98.4 % of Fe_2O_3) plus minor constituents. The Rietveld method quantified the hematite and magnetite species using XRD data and compared them with the Inorganic Crystal Structure Database (ICSD). The XRD data were refined with the HighScore Plus 4.8 software. A calculated diffraction pattern is generated and compared with the observed data using least-squares procedures to minimize the difference between observed data and calculated diffraction patterns. Regarding the mineralogical composition of the flotation feed, the sample is predominantly composed of hematite (97 %) with a low content of magnetite (3 %) plus traces (content < 0.5 %) of gibbsite, goethite and quartz.

Table 2
Chemical composition and mineralogy of the flotation feed.

Mineralogical composition	XRF	Grade (%)
Hematite (97 %)	Fe	68.90
Magnetite (3 %)	SiO_2	0.87
Gibbsite [pp]	Al_2O_3	0.24
Quartz [pp]	P	0.01
Goethite [pp]	Mn	0.04

[pp] possible presence.

Table 3
NaOH volume for different SNMR.

SNMR	The volume of NaOH solution (50 % w/w) used in the gelatinization (μL)	The mass of NaOH used in the gelatinization (g)
3:1	901	0.667
5:1	540	0.400
7:1	386	0.286
9:1	300	0.222

Corn starch (Amidex®3001), supplied by Ingredion Brazil, composed of 25 g/100 g amylose and 75 g/100 g amylopectin, was used as a depressant agent for hematite. Alkyl ether amine 50 % neutralized with acetic acid (Flotigam® 7100), supplied by Clariant - Brazil, was used as a collector. Sodium hydroxide (NaOH), hydrochloric acid (HCl), potassium chloride (KCl), and sodium chloride (NaCl) of analytical grade were purchased from Labsynth, Brazil. They were used to gelatinize starch (NaOH), regulate pH (NaOH, HCl), and act as supporting electrolytes (KCl, NaCl) in the determination of the hydrodynamic diameter of macromolecules and zeta potential measurements. To determine the Hamaker constant of starch films (A_{11}), diiodomethane of analytical grade (Sigma-Aldrich) was used in contact angle measurements. Distilled water (resistivity = 2 MΩ.cm) was employed in flotation tests, whereas Milli-Q® water (resistivity = 18 MΩ.cm) was adopted in all other experiments.

2.2. Starch preparation

Amidex® 3001 (corn starch) is a powder insoluble in cold water, and therefore, it must be gelatinized before being used in any experiment. For constructing a systematic approach to the starch gelatinization, two grams of dry starch were poured into a beaker containing 29 mL of Milli-Q® water (at room temperature) and mixed by a magnetic stirrer for 10 min. After mixing starch in water, different volumes of sodium hydroxide solution (50 % w/w) were added to the mixture to achieve the desired starch:NaOH mass ratio (SNMR) (Table 3). After adding the NaOH solution, the stirring continued for 20 min. The experiments were conducted at the constant room temperature (22–24 °C). Finally, the

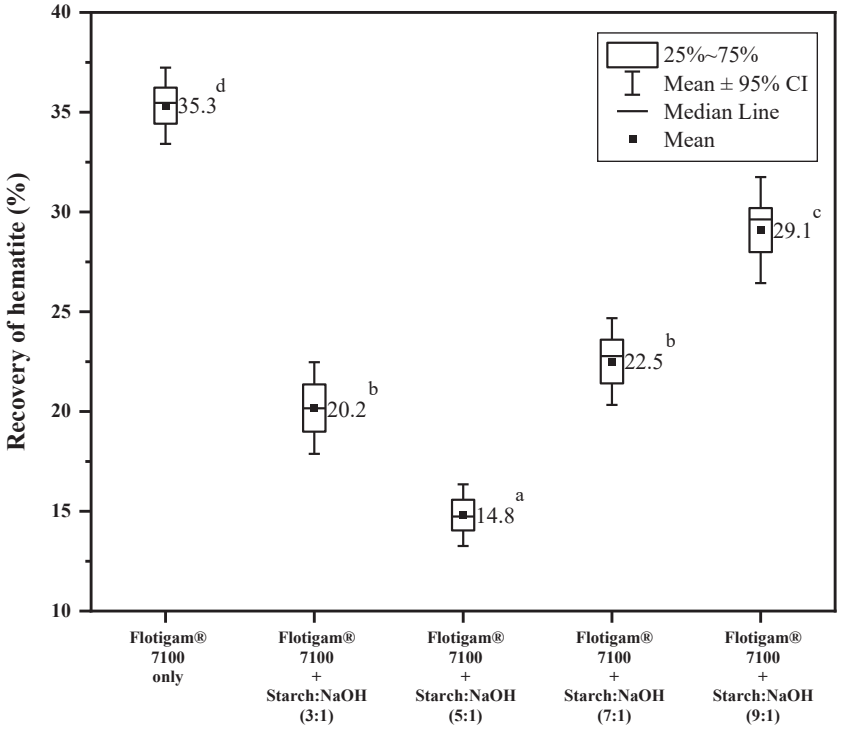

Fig. 1. Recovery of hematite under different SNMR at pH 10.5. Mean values accompanied by different letters are significantly different ($p < 0.05$).

starch gel (6.5 % w/w) was transferred to a 100 mL volumetric flask with the addition of Milli-Q® water to prepare a mother solution (2 % w/w) used in further flotation experiments.

Films of Amidex®3001 gelatinized under different SNMR (3:1, 5:1, and 7:1) were obtained by pouring 10 mL of 1 % w/w gelatinized starch solution in a glass plate left in a vacuum oven (−80 kPa) at 40 °C for 50 h when a dry and whitish thin film was deposited on the plate. The contact angle of the obtained films was used to determine the individual Hamaker constant (A_{11}) of starch prepared at any particular SNMR value.

2.3. Batch flotation

The flotation response of hematite was assessed on the laboratory scale by carrying out flotation experiments at (22 ± 1) °C in a Denver sub-aerated flotation machine endowed with a 1.5L stainless steel cell, operating at 1200 min^{-1} (gas holdup ~ 10 %). The flotation experiments used a gas flow rate (QG) of QG = 27 cm3/s (or 1.6 L/min). A mass of 380 g of hematite was mixed with 700 mL of distilled water to prepare a slurry containing 35.2 % solids (w/w). The pulp was stirred for 1 min, its natural pH was measured (pH = 7.0 ± 0.2), and 175 μL of Amidex® 3001 solution (2 % w/w) – was prepared under different values of SNMR) was poured into the slurry to depress Fe-bearing oxides. After adding NaOH to adjust pH 10.5, the depressant was conditioned for 6 min, followed by adding 7 mL of Flotigam® 7100 (1 % w/w). After 1 min of collector conditioning, the air gauge was opened, and the froth was collected in a tray for 3 min. The floated and sink products were filtered, dried, and weighed. The floatability of hematite (recovery) was calculated based on Eq. (2), where R is the flotation recovery and M_1 and M_2 are the mass of the floated and sunk products, respectively. Each batch of flotation tests was repeated four times.

$$R = \left(\frac{M_1}{M_1 + M_2}\right) \times 100 \quad (2)$$

2.4. Contact angle measurements

Contact angle (θ) measurements were carried out on a basal plane (0 0 1) of a polished section of a hematite chunk by employing the Captive Bubble Method (CBM) in goniometer DSA 25 (supplied by Krüss, Germany) equipped with Advance® software, which allows to measure θ versus time at (22 ± 1) °C. Before any measurement, the mineral surface was carefully cleaned by manual polishing using a nap cloth and a diamond paste (both supplied by Struers, USA) in the presence of pure water for 1 min, ethyl alcohol (analytical grade, 99.5 %) for 1 min and thoroughly washed with Milli-Q® water. After surface cleaning, the hematite sample was conditioned with starch solution (concentration of either 0 or 5 mg/L prepared based on different SNMR) at pH 10.5 for 6 min, followed by Flotigam® 7100 (100 mg/L) conditioning (1 min). After reagent conditioning, the hematite chunk was transferred to a cuvette of high-quality optical glass, which was inserted in the goniometer. For the θ measurements, after particle/bubble contact and adhesion, a baseline was manually adjusted in the three-phase contact point, the Young-Laplace fit was applied to the bubble boundary line, and then, the θ measurement versus time started. All θ measurements were carried out at 22 ± 1 °C during a length of time of 30 min, as the equilibrium contact angle (θ_{eq}) was achieved. Four runs were performed for each experimental condition, and the value of θ_{eq} was the mean value obtained in the last 5 min (600 records). Average equilibrium contact angle ($\overline{\theta}_{eq}$) and standard error were calculated. Single drops of diiodomethane were placed onto the surface of starch films (SNMR of 3:1, 5:1 and 7:1), aiming at measuring the contact angle via Sessile Drop Method (SDM) at (22 ± 1)°C. Although SDM is less accurate and precise than CBM (Tohry et al., 2020), the former was adopted due to the toxicity of diiodomethane. Five runs of 10 min were performed, and the value of θ_{eq} was the mean value obtained in the last 2.5 min (300 records). Average equilibrium contact angle ($\overline{\theta}_{eq}$) and standard error were calculated and used for further statisticala analysis.

2.5. Induction time measurements

As an air bubble adheres to a particle's surface, it experiences a deformation followed by thinning the intervenient water film until its rupture. This way, during the measurement of contact angles, the particle/bubble adherence process was recorded by high-speed photography (USB 3.0 camera - Krüss, Germany). The length of time between the maximum bubble deformation and the beginning of the film liquid rupture (particle and bubble in contact) was considered as the induction time (τ). At least 6 records were analyzed for any experimental condition, and the results were expressed by the arithmetic mean and standard deviation. All the experiments were conducted at (22 ± 1) °C.

2.6. Macromolecules' hydrodynamic diameter

The size distribution of starch colloidal particles was measured by dynamic light scattering (DLS) at Zetasizer Nano - ZS90 (Malvern Instruments Ltd., UK). DLS is a well-established technique for determining the mean size (z-average), polydispersity (PdI), and size distribution of colloidal particles. For DLS measurements, the scattered light from a dispersion containing diffusing particles is correlated with itself, also known as photon correlation spectroscopy. The mean apparent size is then estimated from an intensity-intensity autocorrelation function named $G(\tau)$ (Eq. (3)), which shows a decay rate. $G(\tau)$ is directly related to the Brownian movement of the particles for an ideal experimental scenario (monodisperse system). The exponential decay, as a function of the delay time (t) (Eq. (3)), represents the loss of coherence due to Brownian motion together with the diffusion coefficient (D) and wave vector (q). The signal-to-noise factor (β) expresses the overall optical detection efficiency, also known as the coherence factor or Y-intercept. The relationship between the hydrodynamic diameter (d_H) of a particle and its Brownian movement is defined by the Stokes-Einstein equation (Eq. (4)). The rate of each single-scattering exponential decay function leads to the corresponding translational diffusion coefficient (D) given by the thermal energy (k_BT) divided by the viscous drag of a particle ($3\pi\eta d_H$).

$$G(t) = 1 + \beta\left\{\exp\left(-Dq^2t\right)\right\}^2 \tag{3}$$

$$D = \frac{k_BT}{3\pi\eta d_H} \tag{4}$$

The size distribution was determined for the gelatinized starch solutions at different SNMR (3:1, 5:1, 7:1, or 9:1). For this purpose, 1 mL of starch solution (390–500 mg/L) at pH 10.5 was analyzed in polystyrene cuvettes. All measurements were performed at (22 ± 1) °C, and 0.005 M KCl was added to the starch solutions as a background electrolyte. At least three runs were performed for each experimental condition, and the results were reported as the weighted average ± standard deviation. Since AP macromolecules exhibit larger sizes than those of AM ones (Bello-Perez et al., 1996; Roger et al., 1999; Rolland-Sabaté et al., 2011) (Fig. 1), it is possible to identify size ranges related to both AP and AM species.

2.7. Zeta potential measurements

Zeta potentials of hematite (d_{32} = 6.92 μm) and starch colloidal particles (macromolecules) were determined at pH = 10.5 (22 ± 1 °C) by measuring particles' electrophoretic mobility (Zetasizer-Nano ZS, Malvern Instruments). Regarding hematite, 0.05 g of the mineral was conditioned in 100 mL of NaCl solution (2.4×10^{-2}M) to prepare a 5.0 $\times 10^{-4}$ g mL^{-1} suspension, whose pH 10.5 was adjusted by adding drops of NaOH solution (1 % w/w). Regarding starch dispersions, the product of the gelatinization (a gel containing 68,966 mg/L of starch) was diluted to 20,000 mg/L to prepare a stock solution. A volume of 312.5 μL of the stock solution was diluted to 38 mg/L by adding 164 mL of NaCl solution (2.4×10^{-2}M), whose pH = 10.5 was set by adding drops of a dilute solution of NaOH (1 % w/w). The ionic strength (I = 2.4×10^{-2}M) adopted in the experiments was purposely designed to fit Smoluchowki's equation ($\kappa a > 100$, κ= Debye length; a = particle radius) to convert electrophoretic mobility (μ) to zeta potential (ζ). The inappropriateness of Hückel's equation ($\kappa a < 0.5$) was due to the extremely low ionic strength (I < 4.5×10^{-7} M) of the supporting electrolyte solution necessary to suspend colloidal starch particles of typical radius a = 2.05×10^{-7}m (Table 5). In this case, starch colloidal particles suspended in the very much diluted electrolyte suspension were not detectable (count rate < 10kcps) by Zetasizer Nano ZS-90. In addition, the condition required to use Henry's approach ($0.5 < \kappa a < 100$) was limited to the upper particle radius (a = 5×10^{-8} m) posed by the software of Zetasizer Nano ZS-90.

2.8. Modelling the interaction of colloidal starch and hematite particles

For AP-macromolecules (hereinafter called "starch colloidal particles") to adsorb onto the hematite/water interface via surface complexation (Moreira et al., 2017), both species must be sufficiently close for the reaction accomplishment. This way, the interaction between starch colloidal particles (gelatinized under different SNMR) and hematite's surface was studied by using the classical DLVO theory (Derjaguin and Landau, 1993; Verwey and Overbeek, 1946) by calculating the magnitude of the total energy of interaction (G^{TOT}), which is the sum of G^{LW} and G^{EL}, according to Eq. (1). As maintained by Israelachvili (2011), the Lifshitz-van der Waals energy (G^{LW}) can be assessed by an expression that describes the attractive forces between a sphere (colloidal starch particles) and a plane (hematite's surface). In this system, the non-retarded van der Waals potential energy can be evaluated by the Hamaker approximation of short distances, according to Eq. (5).

$$G^{LW} = -\frac{A_{132}a}{6H} \tag{5}$$

Where:

A_{132} = effective Hamaker constant (J);

a = radius of the colloidal sphere (m);

H = distance between the sphere and the planar surface.

According to Israelachvili (2011), the effective Hamaker constant (A_{132}) can be calculated from the individual Hamaker constants of the three homogeneous phases (A_{11}, A_{22} and A_{33}), according to Eq. (6). In addition, the individual Hamaker constant of starch (A_{11}) can be assessed by Eq. (7).

$$A_{132} = \left(\sqrt{A_{11}} - \sqrt{A_{33}}\right)\left(\sqrt{A_{22}} - \sqrt{A_{33}}\right) \tag{6}$$

$$A_{11} = 24\pi\gamma_s^{LW}(d_0)^2 \tag{7}$$

Where:

γ_s^{LW} = Lifshitz-van der Waals component of the surface energy of media-1;

d_0 = the cut-off distance (1.65×10^{-1} nm);

A_{11}, A_{22} and A_{33} = the Hamaker constants for media-1 (starch), media-2 (hematite), and media-3 (water) interacting with the same medium across a vacuum.

The wettability of a solid surface by a non-polar liquid constitutes an indication of the contribution of Lifshitz-van der Waals energy (γ_s^{LW}) to the total surface energy of the solid (γ_S). This way, a drop of a non-polar liquid (diiodomethane) placed onto the starch/air interface can be used to determine the contact angle and, consequently, the magnitude of γ_s^{LW} by Eq. (8), as maintained by Van Oss (1994).

$$\gamma_L(1 + \cos\theta) = 2\sqrt{\left(\gamma_s^{LW}\gamma_L^{LW}\right)} \tag{8}$$

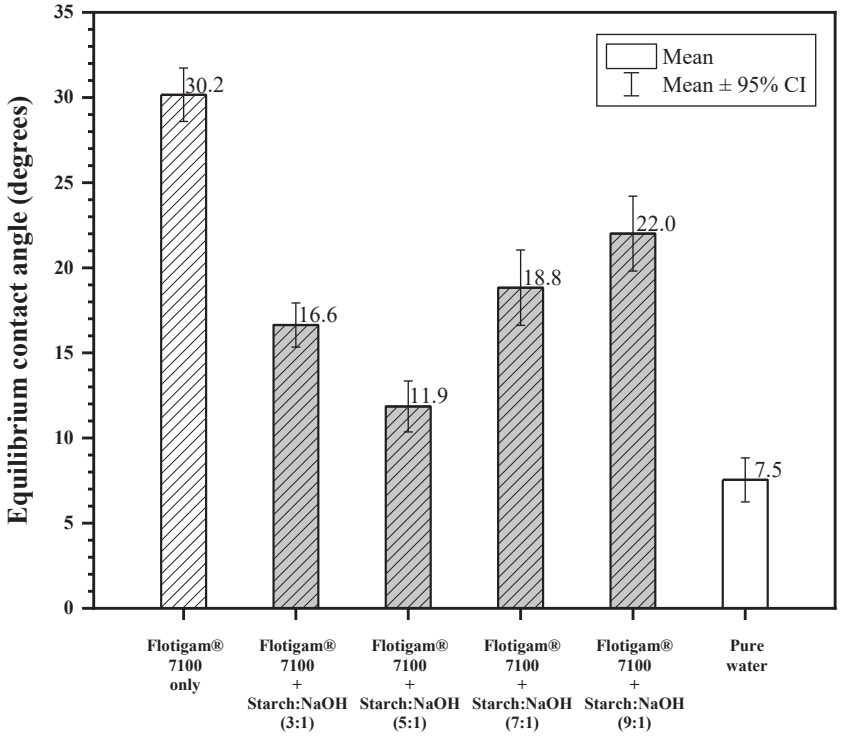

Fig. 2. CBM measured the equilibrium contact angle under different SNMRs at pH 10.5.

Where:

γ_L = total interfacial tension of the apolar liquid (diiodomethane) (J/m^2);

θ = contact angle of a drop of the liquid placed on the solid surface;

γ_L^{LW} = Lifshitz-van der Waals interfacial tension of the apolar liquid (J/m^2).

γ_s^{LW} = Lifshitz-van der Waals interfacial energy of the solid (J/m^2).

The contribution given by the electrostatic interaction energy (G^{EL}) to the total interaction energy (G^{TOT}) can be expressed by Eq. (9). It is related to a system composed of a sphere of radius a interacting with a flat plane (Hunter and White, 1987).

$$G^{EL} = \pi\varepsilon\varepsilon_0 a\left[2\zeta_1\zeta_2\ln\left(\frac{1+e^{-\kappa H}}{1-e^{-\kappa H}}\right) + \left(\zeta_1^2+\zeta_2^2\right)\ln\left(1-e^{-2\kappa H}\right)\right] \quad (9)$$

Where:

ε = dielectric constant of the liquid (ε = 79.6 for water at 22 °C);

ε_0 = electrical permittivity of vacuum ($\varepsilon_0 = 8.85 \times 10^{-12}$ C^{2}J^{-1}m^{-1});

a = radius of the spherical particle (m);

ζ_i = zeta potential (V or J.C^{-1}) of particles suspended in water;

H = separation distance between the sphere and the plane (m);

κ = Debye reciprocal length of the diffuse electrical double layer (m^{-1}), calculated by Eq. (10).

$$\kappa = \left(\frac{2000\Im^2 I}{\varepsilon\varepsilon_0 RT}\right)^{1/2} \quad (10)$$

where $\Im$ = Faraday constant (96,485 C mol^{-1}), I = Ionic strength (2.4×10^{-2} M), T = Absolute temperature (K).

3. Results and discussion

3.1. Batch flotation

For exploring the effect of SNMR on hematite depression through flotation, the low depressant concentration (5 mg/L) coupled with a high collector concentration (100 mg/L) was adopted. This adaptation would highlight the depressant ability of starch based on different SNMRs. Flotation test results (Fig. 1) demonstrated that in the absence of the depressant, the averaged recovery (floatability) of hematite is$R$ = 35.3 %, indicating that ether amine was capable of adsorbing onto hematite/solution interface, promoting hematite hydrophobicity and consequent flotation (Kar et al., 2013; Peres and Correa, 1996; Shrimali et al., 2018; Yang et al., 2023). The flotation outcomes showed that starch could depress hematite, and its depressant ability would depend on the SNMR used in the gelatinization process, which followed the order of SNMR: 5:1 (R = 14.8 %) > 3:1 (R = 20.2 %) > 7:1 (R = 22.5 %) > 9:1 (R = 29.1 %). The mean values recovery for SNMR of 3:1 (R = 20.2 %) and 7:1 (R = 22.5 %) were very close and showed no statistically significant differences ($p < 0.05$), which are accompanied by identical letters as seen in Fig. 1. In the best value of SNMR to accomplish gelatinization (SNMR = 5:1), aiming at accomplishing the most intensive hematite depression (the lowest recovery). These results highlighted that SNMR could markedly play a role in the starch depression and, consequently, in the flotation separation efficiency of hematite.

3.2. Contact angle

Contact angle measurements (θ) results (Fig. 2) showed that hematite exhibited hydrophilic character ($\theta = 7.5°$) in pure water (absence of collector and depressant). Still, it was rendered hydrophobic ($\theta = 30.2°$) in the presence of ether amine solution (100 mg/L) at a basic medium (pH 10.5). However, in the presence of corn starch (5 mg/L) prepared under different SNMR values plus ether amine (100 mg/L), the contact angle of hematite lay in the range $11° < \theta \leq 22°$ indicating that starch was able to hinder collector adsorption onto hematite/solution interface (Shrimali et al., 2018, 2016; Zhu et al., 2022). Moreover, starch gelatinized under the SNMR of 5:1 promoted the lowest value of contact angle ($\theta = 11.9°$), compared to other values of SNMR approached by the experiments: 3:1 ($\theta = 16.6°$), 7:1 ($\theta = 18.8°$) and 9:1 ($\theta = 22.0°$). These results corroborate flotation responses (Fig. 1).

Table 4
Induction time for hematite in different SNMR in the presence of Flotigam® 7100.

SNMR	Induction time (ms) (*)
3:1	44 ± 6^{b}
5:1	55 ± 5^{c}
9:1	29 ± 2^{a}
Flotigam® 7100 only	27 ± 5^{a}

(*) Averaged values accompanied by different letters are significantly different, indicating that they are statistically significant ($p < 0.05$).

Table 5
Size distribution of the starch macromolecules gelatinized under different SNMR.

SNMR	Hydrodynamic diameter of macromolecules (nm) (*)		
	AM	AP	DB
3:1	54 ± 1^{a}	353 ± 6^{a}	Not observed
5:1	75 ± 1^{b}	411 ± 10^{d}	Not observed
7:1	85 ± 6^{c}	380 ± 6^{c}	4991 ± 165
9:1	98 ± 8^{d}	363 ± 10^{b}	5433 ± 128

(*) Averaged values in the same column are accompanied by different Latin letters, indicating that they are statistically significant ($p < 0.05$).

3.3. Induction time

When a particle is in contact with an air bubble, there is an intervening aqueous film between both entities, which delays particle/bubble attachment, and induction time (τ) controls the kinetics of the adhesion process (Fahad et al., 2022; Je et al., 2020; Verrelli et al., 2012; Verrelli and Albijanic, 2015). It was reported that that τ is a more sensitive indicator than θ for predicting mineral floatability (Fahad et al., 2022; Je et al., 2020); in this study, during any θ measurement by the CBM, a high-speed camera filmed the particle/bubble attachment process, aiming at determining the τ magnitude. The τ magnitude assessments (Table 4) depicted that decreasing values of τ vis-à-vis the SNMR used in the starch gelatinization are: τ=55 ms (SNMR = 5:1) > τ=44 ms (SNMR = 3:1) > τ=29 ms (SNMR = 9:1) > τ=27 ms (only collector, in the absence of starch). These results (Fig. 3) indicated that the higher τ, the lower hematite flotability (recovery). This finding showed that starch gelatinization at SNMR = 5:1 promoted the most intensive depression of hematite compared to the other values of SNMR. In general, as starch was gelatinized at SNMR of 5:1, the lowest value of contact angle ($\theta = 11.9°$) coupled with the highest value of induction time ($\tau = 55$ ms) provoked the lowest recovery of hematite ($R = 14.8$ %), indicating that the highest depression was accomplished.

3.4. The size of starch macromolecules after gelatinization

After starch gelatinization under different values of SNMR (3:1, 5:1, 7:1 and 9:1), the size (hydrodynamic diameter) distribution of starch macromolecules was determined by the DLS technique. DLS results indicated (Fig. 4) that curves obtained from starch solutions prepared at SNMR 7:1 and 9:1 exhibited further shoulders positioned within a size range of 3090 nm < d_H < 5560 nm. Those peaks were probably related to debris (DB) resulting from an imperfect gelatinization process. The hydrodynamic diameter (d_H) of starch macromolecules in solution showed a high sensitivity to the NaOH concentration used in the gelatinization process. (Tang et al., 2022) reported that starch granules could swell and rapidly lose molecular weight by alkali-scission at room temperature to form a sol–gel structure in NaOH. The molecular weight reduction could be due to the "peeling" of long-chain starch granules into short-chain remnants through the dissolution of the amylaceous matter promoted by NaOH. This trend showed that the starch macromolecules can become smaller as the concentration of NaOH increases. Results on $\overline{d_H}$ of macromolecules of AM and AP (Table 5) showed that the size of AM macromolecules in solution decreased continuously as the amount of NaOH increased in the gelatinization process, according to the following sequence: $\overline{d_H}$=98 nm (SNMR = 9:1) < $\overline{d_H}$=85 nm (SNMR = 7:1) < $\overline{d_H}$=75 nm (SNMR = 5:1) < $\overline{d_H}$=54 nm (SNMR = 3:1). Regarding the size of AP macromolecules (Table 4), DLS results indicated that $\overline{d_H}$ followed the same trend only when SNMR varied from 5:1 ($\overline{d_H}$ = 411 nm) to 3:1 ($\overline{d_H}$ = 353 nm). In addition, gelatinization conducted at higher values of SNMR (7:1 and 9:1) promoted the occurrence of AP sizes of roughly similar values (360–380 nm). These outcomes suggested that when starch was gelatinized at either SNMR 7:1 or 9:1, the amount of NaOH added to the system was insufficient to fully release

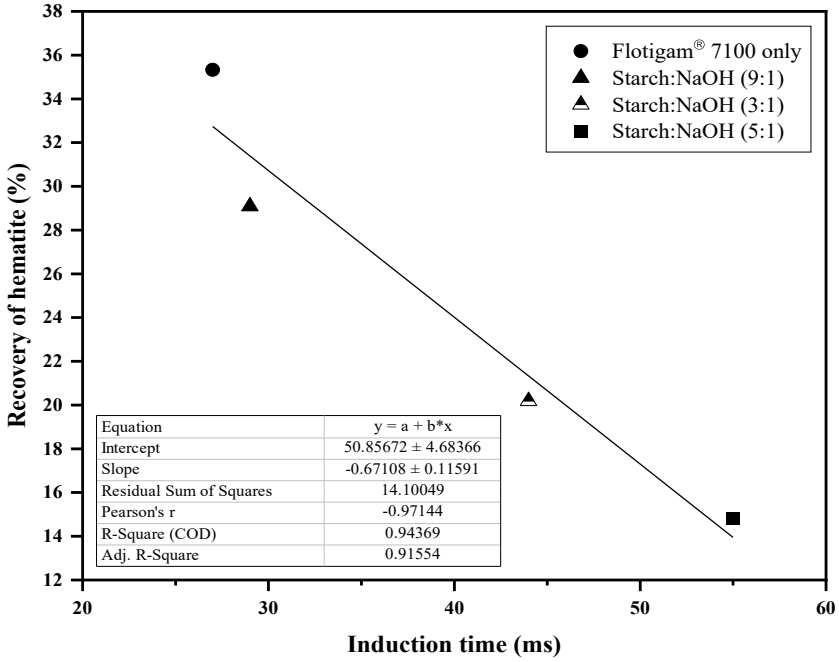

Fig. 3. Recovery of hematite as a function of induction time for different SNMR in the presence of Flotigam® 7100.

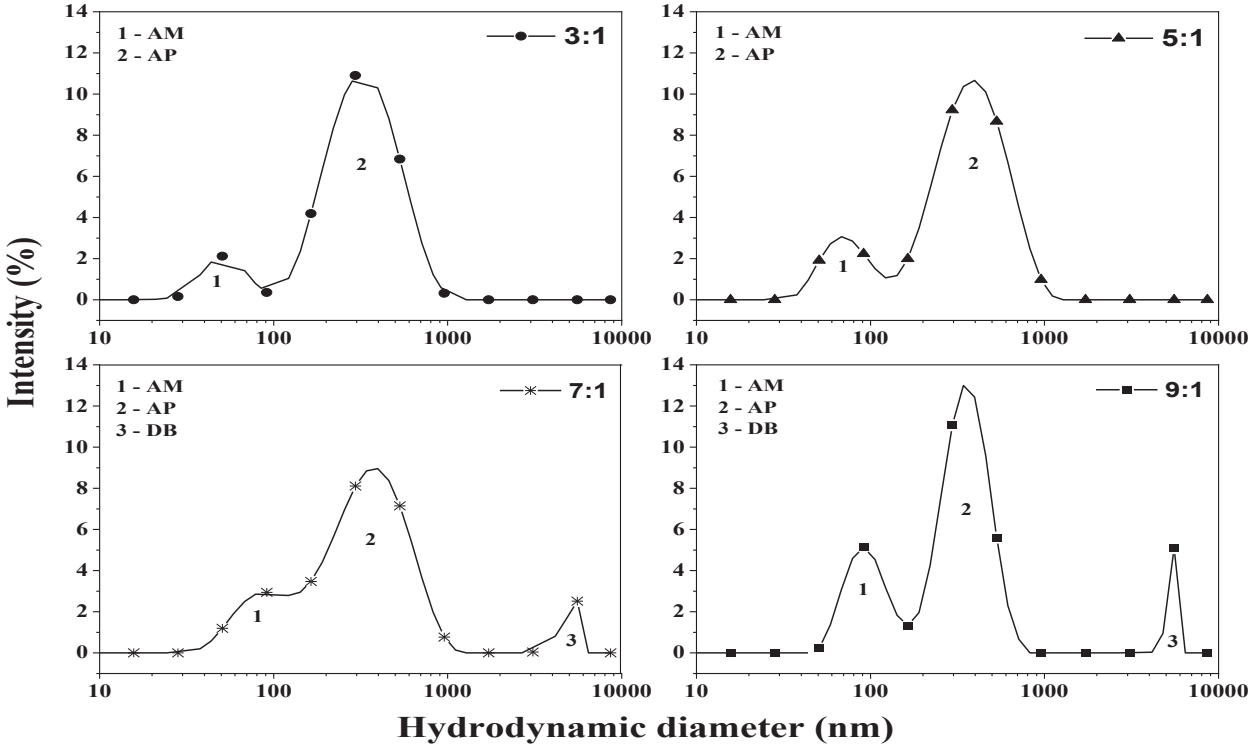

Fig. 4. Frequency versus hydrodynamic diameter of starch macromolecules gelatinized under different SNMR. AM = amylose, AP = amylopectin and DB = debris.

Table 6
The area under the peaks of the starch macromolecules gelatinized under different SNMR.

SNMR	Area under the peaks (% x nm)		
	AM	AP	DB
3:1	81	4639	Not observed
5:1	171	5055	Not observed
7:1	195	4368	2753
9:1	347	3648	2620

the amylaceous matter (AM + AP) to the aqueous solution.

3.5. Particle size, availability of AP-molecules in solution and flotation response of hematite

Once the depression of hematite by starch is promoted by AP-molecules (Iwasaki, 1965), which adsorb onto the hematite/water interface via surface complexation (Weisseborn et al., 1995; Moreira et al., 2017), an enhanced hematite depression is expected to occur as starch gelatinization releases more AP-molecules to the solution. To investigate this possibility, the area under the peaks of frequency (%) versus d_H (nm) (Fig. 4) addressed to AM, AP, and DB were assessed by numerical integration, and the results are displayed in Table 6. Those areas could be regarded as the relative content of AP, AM, and DB in the aqueous solution after the accomplishment of the gelatinization process conducted under SNMR varying from 3:1 to 9:1. Accordingly, the peak areas related to the AP followed the sequence: 5055 %xnm (SNMR = 5:1) > 4639 %xnm (SNMR = 3:1) > 4368 %xnm (SNMR = 7:1) > 3648 %xnm (SNMR = 9:1). Flotation response of hematite (recovery) versus area of AP-peaks showed (Fig. 5a) a significant linear Pearson correlation (r = −0.996), and coefficient of determination (R^2 = 0.99): the higher the area under the AP-Peak, the lower the hematite floatability (low recovery-high depression), corroborating several investigations which maintained that AP macromolecules are the starch component responsible for its depressing action over Fe-bearing minerals (Li et al., 2022; Peres and Correa, 1996; Silva et al., 2016; Yang et al., 2023; Yang and Wang, 2019, 2018). Regarding the relative content of AM in solution, the peak areas related to the AP followed the sequence: 347 %xnm (SNMR = 9:1) > 195 %xnm (SNMR = 7:1) > 171 %xnm (SNMR = 5:1) > 81 %xnm (SNMR = 3:1). The relationship between the hematite floatability and the area under the AM-peaks (Fig. 5b) showed a weakly positive correlation (r = 0.745, R^2 = 0.333), which can be translated as amylose macromolecules do not make a significant contribution to the depressant ability of starch.

3.6. Electrostatic interaction energy between starch colloidal particles and hematite

According to results displayed in Table 7, both hematite (ζ_2 = −29.4 mV) and starch particles (−2mV < ζ_1 < −4mV) are negatively charged at pH = 10.5 (flotation pH). According to Healy and Fuerstenau (1965), the negative interfacial charge exhibited by hematite is predominantly due to the acidic dissociation of surface groups $FeOH_{(surf)}$ to $FeO^-_{(surf)}$, and its isoelectric point lay at 5.9 < pH < 6.7. Zeta potentials exhibited by starch colloidal particles prepared at distinct SNMR (3:1, 5:1, and 7:1) are statistically different ($p < 0.05$): ζ_1 = −4mV (SNMR = 3:1) > ζ_1 = −3mV (SNMR = 5:1) > ζ_1 = −2mV (SNMR = 7:1). In this case, because –OH groups on glucose units behave as very weak acids (11.7 < pK_a < 13.1), its hydrolysis could not be fully responsible for the negative charge developed by starch particles, and the hydrolysis of polymer's end groups cannot be disregarded (Balajee and Iwasaki, 1969; Patai, 1971). The stronger starch gelatinization carried out at SNMR = 3:1, which probably breaks AP-molecules at a larger extent than SNMR = 5:1 and 7:1 (section 3.4), could expose a greater number of hydrolyzable polymer's end groups to solution and consequently, promoting a slight increase in the magnitude of zeta potential of colloidal starch particles.

Values of zeta potential (ζ) and Debye length (κ) displayed in Table 7 were used to calculate the interaction energy due to the electrostatic attraction/repulsion (γ^{EL}) between starch colloidal particles (sphere) and hematite's surface (plane) in the function of the distance sphere/

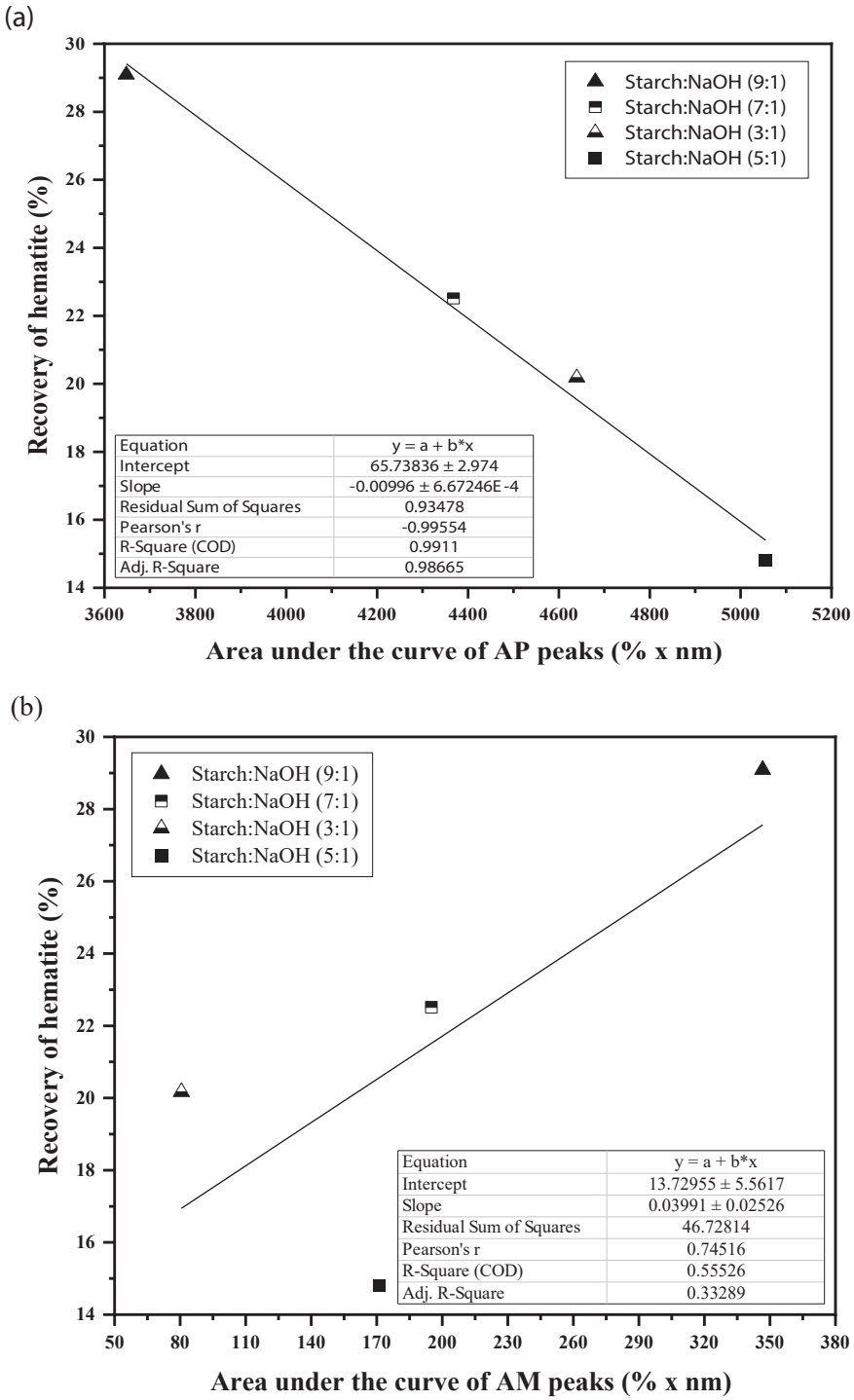

Fig. 5. Recovery of hematite as a function of the area under the curves of (a) AP peaks and (b) AM peaks in solution after gelatinization.

Table 7
Zeta potential of hematite and starch colloidal particles at pH = 10.5 suspended in NaCl solution (2.4×10^{-2}M).

Phases	$\kappa(m^{-1})$	Zeta potential (mV)
Hematite	5.12×10^{8}	-29.36 ± 0.44
Starch (SNMR = 3:1)	(**)	-3.61 ± 0.10^{a}
Starch (SNMR = 5:1)		-2.82 ± 0.09^{b}
Starch (SNMR = 7:1)		-2.31 ± 0.06^{c}

(*) Used as supporting electrolyte; (**) Calculated by Eq. (10).

Table 8
Electrostatic energy interaction between a sphere (starch colloidal particle) and a plane (hematite surface) versus the separation distance (H).

H (nm)	$G^{EL}(10^{-21}$ J)		
	3:1	5:1	7:1
2.5	19.8 ± 1.3	11.2 ± 1.4	3.2 ± 0.9
5.0	10.8 ± 0.4	9.3 ± 0.4	6.7 ± 0.2
10.0	1.0 ± 0.0	0.9 ± 0.0	0.7 ± 0.0

Table 9
Parameters used to calculate the Hamaker constant of starch (A_{11}).

SNMR	Contact angle (degree)	γ_L(mJ/m^2)	γ_L^{LW}(mJ/m^2)	γ_S^{LW}(mJ/m^2)
3:1	31.38 ±0.08 [a]	50.8	50.8	43.6 4 ± 0. 03
5:1	38.2 2 ± 0.10 [b]	(Van Oss, 1994)	(Van Oss, 1994)	40.49 ±0. 05
7:1	38.87 ±0.08 [b]			40.17 ±0. 04

Table 10
The Hamaker constant of starch (A_{11}), hematite (A_{22}), water (A_{33}), and effective (A_{132}).

SNMR	Hamaker constant (10^{-20} J)			
	A_{11}	A_{22}	A_{33}	A_{132}
3:1	8.96 ± 0.01	25.0	3.7	3.29 ± 0.00
5:1	8.31 ± 0.01			2.95 ± 0.01
7:1	8.25 ± 0.01	(Lins et al., 1995)	(Van Oss, 1994)	2.92 ± 0.01

plane (H), according to Eq. (9). Since the length of the electrical double layer (κ^{-1}) of both sphere and plane is approximately 2 nm, the distances considered in the calculation of G^{EL} varied from 2.5 nm to 10 nm. According to the results displayed in Table 8, the modulus of G^{EL} increases as the sphere gets closer to the plane, and the strictly positive sign ($G^{EL} > 0$) indicates the existence of electrostatic repulsion between the sphere and the plane throughout the explored range of distances ($2.5 \leq H \leq 10.0$ nm). Furthermore, in Table 8, at any distance (H) from the hematite's surface (plane), starch colloidal particles (sphere) prepared at SNMR = 3:1 are more intensively repelled from the surface than those prepared at either SNMR = 5:1 or SNMR = 7:1. This trend is certainly due to differences in the magnitude/sign of zeta potential of starch particles versus SNMR displayed in Table 7.

3.7. Lifshitz-van der Waals interaction energy between colloidal starch and hematite

Results from measurements of contact angle (Table 9) via the Sessile Drop Method (SDM) were obtained by placing a drop of the non-polar liquid diiodomethane ($\gamma_L = \gamma_L^{LW} = 50.8$ mJ/m^2) onto the surface of starch films gelatinized at different SNMR (3:1 × 5:1 × 7:1). As displayed in Table 9, starch films gelatinized at SNMR = 3:1 showed a lower contact angle ($\theta = 31°$) than those prepared at SNMR = 5:1 and SNMR = 7:1 (θ = 38-39°), which are statistically similar ($p < 0.05$). The significant difference observed in the value of contact angle indicates that starch films gelatinized at SNMR = 3:1 are more wetted by the non-polar liquid than those gelatinized at SNMR = 5:1 and SNMR = 7:1. A greater wettability of a solid (starch film) by a non-polar liquid (diiodomethane) indicates a more intensive solid/liquid interaction favored by Lifshitz-van der Waals forces, a phenomenon associated with the Lifshitz-van der Waals component of the interfacial energy of the starch film (γ_S^{LW}) and the non-polar liquid (γ_L^{LW}). According to results presented in Table 9, starch films gelatinized at SNMR = 3:1 exhibit higher γ_S^{LW} (43.64 mJ/m^2) than those gelatinized at SNMR = 5:1 (40.49 mJ/m^2) and SNMR = 7:1 (40.17 mJ/m^2), which are inferred as similar (confidence interval of 95 %).

Values of γ_S^{LW} related to starch films gelatinized with different SNMR (3:1 × 5:1 × 7:1) were used to assess their respective individual Hamaker constants (A_{11}) and, consequently, the effective Hamaker constant of the interaction starch/hematite in aqueous medium (A_{132}). According to results displayed in Table 10, the value of both Hamaker constants (A_{11} and A_{132}) related to starch prepared at SNMR = 3:1 is greater than those values related to the gelatinization accomplished at SNMR = 5:1 and SNMR = 7:1, which are inferred as similar (confidence interval of 95 %). The information displayed in Table 5 (hydrodynamic diameter of starch colloidal particles after gelatinization) and Table 10 (values of A_{132}) were taken to Eq. (5) to assess the magnitude of the Lifshitz-van der Waals (G^{LW}) attractive energy between starch (sphere) and hematite surface (flat plane) at distances (H) from the hematite's surface varying from 2 nm to 20 nm. The results are depicted in Fig. 6, where the magnitude of G^{LW} increases exponentially as the distance (H) between the sphere (starch colloidal particle) and the plane (hematite's surface) decreases from 20 nm to 2 nm. In Fig. 6, at any distance from the plane, one observes the following sequence of attractive energy (G^{LW}): SNMR = 5:1 > SNMR = 3:1 > SNMR = 7:1. Considering the magnitude of A_{132}, one would expect that colloidal starch particles prepared at SNMR = 3:1 ($A_{132} = 3.29 \times 10^{-20}$ J) would be more

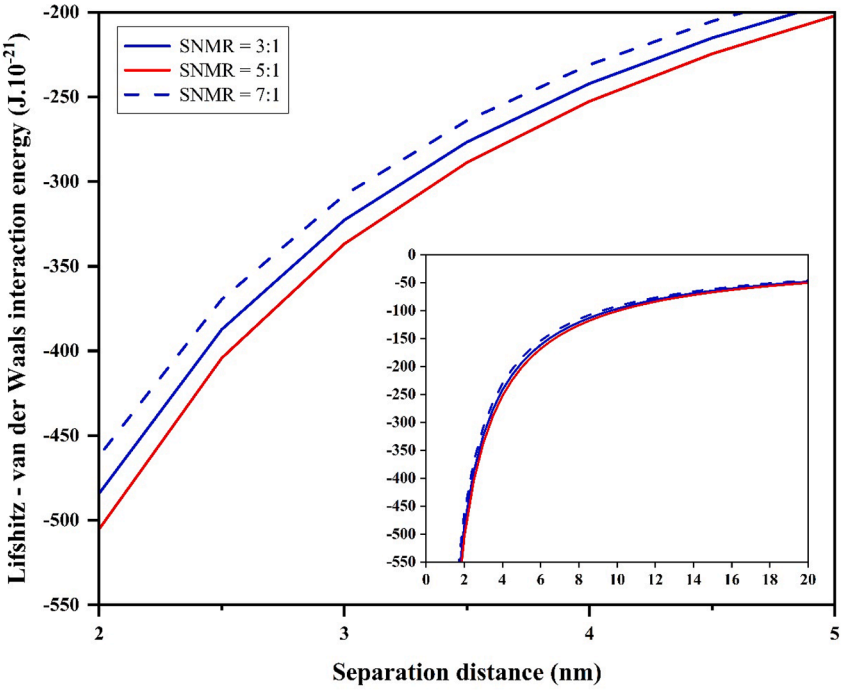

Fig. 6. Lifshitz-van der Waals interaction energy of starch (sphere) and hematite's surface (plane) versus the separation distance (pH = 10.5, 22 ±1 °C).

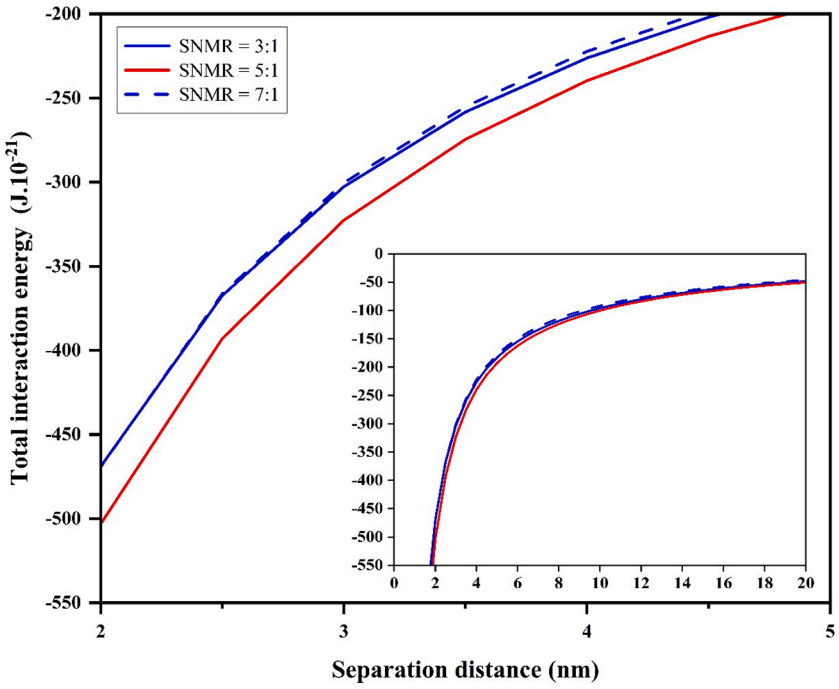

Fig. 7. Total interaction energy between starch (sphere) and hematite's surface (plane) versus the separation distance (pH = 10.5, 22 ±1 °C).

Table 11
Interaction energy (G^{LW}, G^{EL}, G^{TOT}) between starch colloidal particles and hematite's surface x separation distance (H).

Energy (10^{-21} J)	H = 5 nm 3:1	5:1	7:1	H = 10 nm 3:1	5:1	7:1
G^{LW}	−193.6 ± 1.8	−202.0 ± 2.7	−184.6 ± 1.6	−96.8 ± 0.9	−101.0 ± 1.4	−92.3 ± 0.8
G^{EL}	+10.8 ± 0.4	+9.3 ± 0.4	+6.7 ± 0.2	+1.0 ± 0.0	+0.9 ± 0.0	+0.7 ± 0.0
G^{TOT}	−182.8 ± 1.9	−192.7 ± 2.9	−177.9 ± 1.6	−96.7 ± 0.9	−100.1 ± 1.4	−91.6 ± 0.8

intensively attracted to hematite's surface than starch colloidal particles gelatinized with SNMR = 5:1 ($A_{132} = 2.95 \times 10^{-20}$ J) or 7:1 ($A_{132} = 2.92 \times 10^{-20}$ J). However, according to Eq. (5), the attractive Lifshitz-van der Waals interaction energy (G^{LW}) depends not only on A_{132} but also on particle radius (a). According to results presented in Table 5, starch colloidal particles (AP-peak) gelatinized with SNMR = 5:1 exhibit the largest hydrodynamic diameter ($\overline{d_H}$ = 411 nm) compared to SNMR = 3:1 ($\overline{d_H}$ = 353 nm) and SNMR = 7:1 ($\overline{d_H}$ = 380 nm). Because the particle radius (a) is the half of d_H, the results depicted in Fig. 6 (G^{LW}) and Table 10 (A_{132}) indicate that the size of the starch colloidal particles yielded by the gelatinization process exerts a stronger and decisive influence on the Lifshitiz-van der Waals attractive energy (G^{LW}) between starch and hematite.

3.8. Total interaction energy between colloidal starch and hematite

The total energy of interaction (G^{TOT}) between starch colloidal particles (sphere) and hematite's surface (plane) in function of the separation distance (H) was calculated by Eq. (1), and results are depicted in Fig. 7, where one observes a lack of any energy barrier between the sphere and the plane throughout the explored range of separation distance (2–20 nm). For the purpose of comparison, values of G^{LW}, G^{EL} and G^{TOT} calculated at separation distances of H = 5 nm × H = 10 nm are displayed in Table 11, where one observes that electrostatic repulsion ($G^{EL} > 0$) between the sphere (starch colloidal particles) and the plane (hematite's surface) is very much lower than the attraction ($G^{LW} < 0$) promoted by Lifshitz-van der Waals forces. Results depicted in Fig. 7 also indicate that starch colloidal particles are attracted to the surface of hematite ($G^{TOT} < 0$) throughout the explored range of distances (2–20 nm), regardless of the SNMR used in the gelatinization. However, the gelatinization carried out at SNMR = 5:1 promoted the most intensive attraction. Statistical analysis of results of G^{TOT} calculated at H = 2.0 nm (Fig. 8) indicate that G^{TOT} related to starch gelatinization at SNMR = 5:1 (-502.9×10^{-21} J) is greater than G^{TOT} calculated for starch prepared at SNMR = 3:1 (-468.8×10^{-21} J) and SNMR = 7:1 (-469.0×10^{-21} J), at a confidence level of 95 %. These results corroborate the more intensive depression of hematite (flotation recovery) by starch prepared at SNMR = 5:1, compared to SNMR = 3:1 and SNMR = 7:1 (Fig. 1), influenced by the lowest contact angle (Fig. 2) and the highest induction time (Fig. 3).

4. Conclusions

A successful hematite concentration through the reverse cationic flotation separation from quartz demands hematite depression, which has been accomplished around the world by using starch. Raw starch must be gelatinized before flotation to release its active matter (amylopectin macromolecules) to the flotation solution, allowing starch/hematite interaction and consequently promoting hematite depression. This study explored the influence of the starch/NaOH mass ratio (SNMR) used in starch gelatinization on the hematite flotation response (depression). Reverse flotation results indicated that SNMR tremendously affects the starch depression capabilities and the flotation responses. The lowest hematite floatability ($R = 14.8$ %) was observed at SNMR = 5:1, which could be linked to the lowest contact angle ($\theta = 11.9°$) and the highest induction time (τ = 55 ms). Those outcomes demonstrated that the higher hematite depression efficiency of the SNMR = 5:1 results from a slower particle/bubble attachment (higher induction time) process coupled with fewer hydrophobic particles (lower contact angle). The higher effective depression of hematite attained at SNMR = 5:1 compared to the other values of SNMR (3:1, 7:1, and 9:1) was potentially due to a complete release of AP and AM macromolecules into the aqueous solution, characterized by the lack of debris (observed solely at SNMR of 7:1 and 9:1), which coupled with

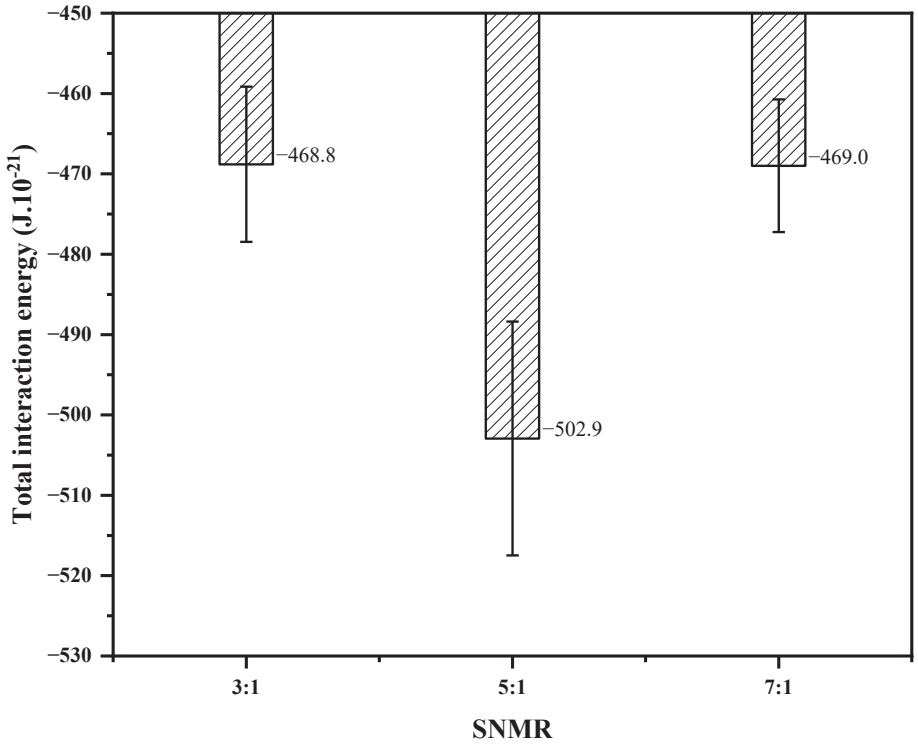

Fig. 8. The influence of SNMR used in starch gelatinization on the total interaction energy (G^{TOT}) between starch (sphere) and hematite's surface at H = 2 nm (pH = 10.5, 22 ±1 °C).

greater availability of AP macromolecules in solution. In addition, starch prepared at SNMR = 5:1 released AP macromolecules to the solution with greater hydrodynamic diameter ($\overline{d_H}$ = 411 nm) than those released by the gelatinization conducted under SNMR = 3:1 ($\overline{d_H}$ = 353 nm). The recovery of hematite showed strong correlations (r = −0.996 and R^2 = 0.99) with the areas under the peaks related to the presence of AP in solution, indicating the higher availability of AP macromolecules to adsorb onto hematite/water interface. The interaction between hematite and colloidal starch particles (AP-macromolecules) was approached by the classical DLVO theory to assess the total energy of interaction (G^{TOT}) versus the separation distance between a plane (hematite's surface) and a sphere (starch colloidal particle) in aqueous medium (at pH = 10.5, temperature = 22 °C). Since G^{TOT} is the sum of Lifshitz-van der Waals attractive energy (G^{LW}) plus the electrostatic (G^{EL}) attractive/repulsive energy, the magnitude and sign of both contributions (G^{LW}, G^{EL}) were assessed. The magnitude of G^{LW} was assessed based on the wettability of starch films (prepared at SNMR of 3:1 × 5:1 × 7:1) by a non-polar liquid (diiodomethane), which allowed the assessment of the individual Hamaker constants of starch (8×10^{-20}J < A_{11} < 9×10^{-20}J) gelatinized at different SNMR (3:1 × 5 × 1 × 7:1). The individual Hamaker constants of water (A_{33}) and hematite (A_{22}) were found in literature. Based on A_{11}, A_{22}, and A_{33}, the effective Hamaker constant of the starch/water/hematite system (A_{132}) was finally calculated: 2.9×10^{-20}J < A_{132} < 3.3×10^{-20}J. In addition, the magnitude of G^{EL} was calculated based on the zeta potential of starch (−2mV < ζ_1 < −4mV) and hematite (ζ_2 = −29 mV) at pH = 10.5 and Debye length of κ = 5.12×10^8 m^{-1}. Results indicated that starch colloidal particles (sphere) are attracted (G^{TOT} < 0) to the surface of hematite (plane) throughout the explored range of distances (2–20 nm), regardless of the SNMR used in the gelatinization. However, the gelatinization carried out at SNMR = 5:1 promoted the most intensive attraction. Statistical analysis of results for G^{TOT} calculated at H = 2.0 nm indicate that G^{TOT} related to starch gelatinization at SNMR = 5:1 (-502.9×10^{-21} J) is greater than G^{TOT} calculated for starch prepared at SNMR = 3:1 (-468.8×10^{-21} J) and SNMR = 7:1 (-469.0×10^{-21} J), at a confidence level of 95 %. These results corroborate the more intensive hematite depression by starch prepared at SNMR = 5:1 compared to the other values explored by this study.

CRediT authorship contribution statement

Elaine Cristina Andrade: Writing – original draft, Methodology, Investigation, Formal analysis, Data curation, Conceptualization. **Saeed Chehreh Chelgani:** Writing – review & editing, Writing – original draft, Visualization, Validation, Methodology, Investigation, Formal analysis, Conceptualization. **Laurindo de Salles Leal Filho:** .

Declaration of competing interest

The authors declare that they have no known competing financial interests or personal relationships that could have appeared to influence the work reported in this paper.

Data availability

Data will be made available on request.

Acknowledgments

The authors acknowledge the Vale S.A. for kindly donating the hematite sample used in this study. Author Elaine C. Andrade acknowledges the Coordination for the Improvement of Higher Education Personnel (CAPES) for providing a doctoral scholarship. Saeed Chehreh Chelgani was funded by the CAMM-green flotation work package.

References

Asimi Neisiani, A., Saneie, R., Mohammadzadeh, A., Wonyen, D.G., Chehreh Chelgani, S., 2023. Biodegradable hematite depressants for green flotation separation – An overview. Miner. Eng. 199, 108114 https://doi.org/10.1016/j.mineng.2023.108114.

Balajee, S.R., Iwasaki, I., 1969. Adsorption mechanism of starches in flotation and flocculation of iron ores. Trans. Am. Inst. Min. Metall. Eng. 244, 401–406.
Bello-Perez, L.A., Paredes-Lopez, O., Roger, P., Colona, P., 1996. Molecular characterization of some amylopectins. Cereal Chem. 73, 12–17.
Botero, A.E.C., Torem, M.L., De Mesquita, L.M.S., 2008. Surface chemistry fundamentals of biosorption of Rhodococcus opacus and its effect in calcite and magnesite flotation. Miner. Eng. 21, 83–92. https://doi.org/10.1016/j.mineng.2007.08.019.
Cornell, H.J., 1963. The effect of amylopectin on the properties of starch gels. Starch/stärke 15, 43–50. https://doi.org/10.1002/star.19630150202.
Deng, J., Yang, S., Liu, C., Li, H., 2019. Effects of the calcite on quartz flotation using the reagent scheme of starch/dodecylamine. Colloids Surf., A Physicochem. Eng. Asp. 583, 123983 https://doi.org/10.1016/j.colsurfa.2019.123983.
Derjaguin, B., Landau, L., 1993. Theory of the stability of strongly charged lyophobic sols and of the adhesion of strongly charged particles in solutions of electrolytes. Prog. Surf. Sci. 43, 30–59. https://doi.org/10.1016/0079-6816(93)90013-L.
Fahad, M.K., Prakash, R., Majumder, S.K., Ghosh, P., 2022. Investigation of the induction time and recovery in a flotation column: A kinetic analysis. Sep. Sci. Technol. 57, 2937–2954. https://doi.org/10.1080/01496395.2022.2084629.
Félix, L.L., Moreira, G.F., Filho, L.S.L., Stavale, F., 2022. Starch adsorption on hematite surfaces: Evidence of the adsorption mechanism dependence on the surface orientation. Miner. Eng. 178, 107429 https://doi.org/10.1016/j.mineng.2022.107429.
Fu, X., Gao, Y., Han, H., Gao, Z., Wang, L., Sun, W., Yue, T., 2022. Quantization of the hydration and dodecylamine adsorption characteristics of hematite and quartz surface active sites to forecast the flotation behavior of minerals. Miner. Eng. 183, 107571 https://doi.org/10.1016/j.mineng.2022.107571.
Healy, T.W., Fuerstenau, D.W., 1965. The oxide-water interface-interrelation of the zero point of charge and the heat of immersion. J. Colloids Sci. 20, 376–386.
Hunter, R.J., White, L.R., 1987. Foundations of Colloid Science, Oxford Science Publications. Clarendon Press ; Oxford University Press, Oxford [Oxfordshire] : New York.
Iselau, F., Phan Xuan, T., Matic, A., Persson, M., Holmberg, K., Bordes, R., 2016. Competitive adsorption of amylopectin and amylose on cationic nanoparticles: a study on the aggregation mechanism. Soft Matter 12, 3388–3397. https://doi.org/10.1039/C6SM00165C.
Israelachvili, J.N., 2011. Intermolecular and Surface Forces, 3rd ed. Academic press, Burlington (Mass.).
Iwasaki, I., 1965. Interaction of starch and calcium in soap flotation of activated silica from iron ores. Trans. Am. Inst. Min. Metall. Pet. Eng. 232, 383–387.
Je, J., Kwon, J., Cho, H., 2020. Simulation of bubble–plate attachment and estimation of induction time using smoothed particle hydrodynamics. Miner. Eng. 149, 106227 https://doi.org/10.1016/j.mineng.2020.106227.
Kar, B., Sahoo, H., Rath, S.S., Das, B., 2013. Investigations on different starches as depressants for iron ore flotation. Miner. Eng. 49, 1–6. https://doi.org/10.1016/j.mineng.2013.05.004.
Laskowski, J.S., Liu, Q., O'Connor, C.T., 2007. Current understanding of the mechanism of polysaccharide adsorption at the mineral/aqueous solution interface. Int. J. Miner. Process. 84, 59–68. https://doi.org/10.1016/j.minpro.2007.03.006.
Li, K., Zhang, H., Peng, T., Liu, C., Yang, S., 2022. Influences of starch depressant with the various molecular structure on the interactions between hematite particles and flotation bubbles. Colloids Surf., A Physicochem. Eng. Asp. 652, 129814 https://doi.org/10.1016/j.colsurfa.2022.129814.
Lins, F.F., Middea, A., Adamian, R., 1995. Processing of hydrophobic minerals and fine coal. In: Proceedings of the First UBC-McGill Bi-Annual International Symposium on Fundamentals of Mineral Processing. Presented at the Proceedings of the First UBC-McGill Bi-Annual International Symposium on Fundamentals of Mineral Processing, p. 61.
Moreira, G.F., Peçanha, E.R., Monte, M.B.M., Leal Filho, L.S., Stavale, F., 2017. XPS study on the mechanism of starch-hematite surface chemical complexation. Miner. Eng. 110, 96–103. https://doi.org/10.1016/j.mineng.2017.04.014.
Nykänen, V.P.S., Braga, A.S., Pinto, T.C.S., Matai, P.H.L.S., Lima, N.P., Leal Filho, L.S., Monte, M.B.M., 2020. True flotation *versus* entrainment in reverse cationic flotation for the concentration of iron ore at industrial scale. Miner. Process. Extr. Metall. Rev. 41, 11–21. https://doi.org/10.1080/08827508.2018.1514298.
Patai, S., 1971. The Chemistry of the Hydroxyl Group, The Chemistry of Functional Groups. Interscience, London, New York.
Peres, A.E.C., Correa, M.I., 1996. Depression of iron oxides with corn starches. Miner. Eng. 9, 1227–1234. https://doi.org/10.1016/S0892-6875(96)00118-5.
Pinto, C.L.L., De Araujo, A.C., Peres, A.E.C., 1992. The effect of starch, amylose and amylopectin on the depression of oxi-minerals. Miner. Eng. 5, 469–478. https://doi.org/10.1016/0892-6875(92)90226-Y.
Ragheb, R., Nobbmann, U., 2020. Multiple scattering effects on intercept, size, polydispersity index, and intensity for parallel (VV) and perpendicular (VH) polarization detection in photon correlation spectroscopy. Sci Rep 10, 21768. https://doi.org/10.1038/s41598-020-78872-4.
Roger, P., Bello-Perez, L.A., Colonna, P., 1999. Contribution of amylose and amylopectin to the light scattering behaviour of starches in aqueous solution 40, 6897–6909.
Rohem Peçanha, E., Da Fonseca De Albuquerque, M.D., Antoun Simão, R., De Salles Leal Filho, L., De Mello Monte, M.B., 2019. Interaction forces between colloidal starch and quartz and hematite particles in mineral flotation. Colloids Surf., A: Physicochem. Eng. Aspects 562, 79–85. 10.1016/j.colsurfa.2018.11.026.
Rolland-Sabaté, A., Guilois, S., Jaillais, B., Colonna, P., 2011. Molecular size and mass distributions of native starches using complementary separation methods: Asymmetrical Flow Field Flow Fractionation (A4F) and Hydrodynamic and Size Exclusion Chromatography (HDC-SEC). Anal. Bioanal. Chem. 399, 1493–1505. https://doi.org/10.1007/s00216-010-4208-4.
Shrimali, K., Jin, J., Hassas, B.V., Wang, X., Miller, J.D., 2016. The surface state of hematite and its wetting characteristics. J. Colloid Interface Sci. 477, 16–24. https://doi.org/10.1016/j.jcis.2016.05.030.
Shrimali, K., Atluri, V., Wang, Y., Bacchuwar, S., Wang, X., Miller, J.D., 2018. The nature of hematite depression with corn starch in the reverse flotation of iron ore. J. Colloid Interface Sci. 524, 337–349. https://doi.org/10.1016/j.jcis.2018.04.002.
Shrimali, K., Miller, J.D., 2016. Polysaccharide depressants for the reverse flotation of iron ore. Trans. Indian Inst. Met. 69, 83–95. https://doi.org/10.1007/s12666-015-0708-4.
Silva, E.M.S., Peres, A.E.C., Silva, A.C., Florêncio, D.L., Caixeta, V.H., 2019. Sorghum starch as depressant in mineral flotation: part 2 – flotation tests. J. Mater. Res. Technol. 8, 403–410. https://doi.org/10.1016/j.jmrt.2018.04.002.
Silva, A.C., Sousa, D.N., Silva, E.M.S., Fontes, T.P., Tomaz, R.S., 2016. Optimal consume of NaOH in starches gelatinization for froth flotation. World Acad. Sci. Eng. Technol. Int. J. Environ. Ecol. Eng. 10, 994–999.
Silva, A.C., Silva, E.M.S., Peres, A.E.C., Sousa, D.N., 2017. Temperature influence in cornstarch gelatinization for froth flotation. REM. Int. Eng. J. 70, 231–235. https://doi.org/10.1590/0370-44672016700085.
Silva, A.C., Sousa, D.N., Silva, E.M.S., 2021. Hematite and quartz microflotation using millet starch as depressant. REM. Int. Eng. J. 74, 107–116. https://doi.org/10.1590/0370-44672020740090.
Tang, M., Liu, Q., 2012. The acidity of caustic digested starch and its role in starch adsorption on mineral surfaces. Int. J. Miner. Process. 112–113, 94–100. https://doi.org/10.1016/j.minpro.2012.06.001.
Tang, M., Wen, S., Liu, D., 2016. Effects of heating- or caustic-digested starch on its flocculation on hematite. Miner. Process. Extr. Metall. Rev. 37, 49–57. https://doi.org/10.1080/08827508.2015.1115986.
Tang, M., Wang, Y., Niu, X., Liu, D., 2022. Morphological characteristics of starch sol-gel and its influences on flocculation of fine particles. Miner. Eng. 186, 107745 https://doi.org/10.1016/j.mineng.2022.107745.
Tohry, A., Dehghan, R., Vale Oliveira, A., Chehreh Chelgani, S., Filho, D.S.L., L.,, 2020. Enhanced Washburn Method (EWM): A comparative study for the contact angle measurement of powders. Adv. Powder Technol. 31, 4665–4671. https://doi.org/10.1016/j.apt.2020.10.014.
Van Oss, C.J., 1994. Interfacial Forces in Aqueous Media. M. Dekker, New York Basel Hong Kong.
Verrelli, D.I., Albijanic, B., 2015. A comparison of methods for measuring the induction time for bubble–particle attachment. Miner. Eng. 80, 8–13. https://doi.org/10.1016/j.mineng.2015.06.011.
Verrelli, D.I., Koh, P.T.L., Bruckard, W.J., Schwarz, M.P., 2012. Variations in the induction period for particle–bubble attachment. Miner. Eng. 36–38, 219–230. https://doi.org/10.1016/j.mineng.2012.03.034.
Verwey, E.J.W., Overbeek, J.T.G., 1946. Long distance forces acting between colloidal particles. Trans. Faraday Soc. 42, B117. https://doi.org/10.1039/tf946420b117.
Weisseborn, P.K., Warren, L.J., Dunn, J.G., 1995. Selective flocculation of ultrafine iron ore. 1. Mechanism of adsorption of starch onto hematite. Colloids Surf., A Physicochem. Eng. Asp. 99, 11–27. https://doi.org/10.1016/0927-7757(95)03111-P.
Yang, S., Li, C., Wang, L., 2017. Dissolution of starch and its role in the flotation separation of quartz from hematite. Powder Technol. 320, 346–357. https://doi.org/10.1016/j.powtec.2017.07.061.
Yang, S., Wang, L., 2018. Structural and functional insights into starches as depressant for hematite flotation. Miner. Eng. 124, 149–157. https://doi.org/10.1016/j.mineng.2018.05.022.
Yang, S., Wang, L., 2019. Measurement of froth zone and collection zone recoveries with various starch depressants in anionic flotation of hematite and quartz. Miner. Eng. 138, 31–42. https://doi.org/10.1016/j.mineng.2019.04.027.
Yang, S., Xu, Y., Kang, H., Li, K., Li, C., 2023. Investigation into starch adsorption on hematite and quartz in flotation: Role of starch molecular structure. Appl. Surf. Sci. 623, 157064 https://doi.org/10.1016/j.apsusc.2023.157064.
Zhang, M., Xu, Z., Wang, L., 2022. Ultrasonic treatment improves the performance of starch as depressant for hematite flotation. Ultrason. Sonochem. 82, 105877 https://doi.org/10.1016/j.ultsonch.2021.105877.
Zhu, Z., Li, Z., Yin, W., Yang, B., Qu, J., Zhang, N., Chen, S., Yu, Y., Chang, J., Liu, L., 2022. Snap-in interactions between water droplets and hematite/quartz surfaces with various roughness after conditioning with soluble starch and DDA using a dynamic microbalance. Miner. Eng. 177, 107358 https://doi.org/10.1016/j.mineng.2021.107358.